Atomistic simulations of dislocation processes in copper

2002 J. Phys.: Condens. Matter 14 2929

(http://iopscience.iop.org/0953-8984/14/11/309)

INSTITUTE OF PHYSICS PUBLISHING JOURNAL OF PHYSICS: CONDENSED MATTER

J. Phys.: Condens. Matter **14** (2002) 2929–2956 PII: S0953-8984(02)28394-0

Atomistic simulations of dislocation processes in copper

Tejs Vegge[1,2] **and Karsten W Jacobsen**[1]

[1] Center for Atomic-scale Materials Physics and Department of Physics, Technical University of Denmark, DK-2800 Kongens Lyngby, Denmark
[2] Materials Research Department, Risø National Laboratory, DK-4000 Roskilde, Denmark

E-mail: vegge@fysik.dtu.dk

Received 30 August 2001, in final form 20 November 2001
Published 8 March 2002
Online at stacks.iop.org/JPhysCM/14/2929

Abstract

We discuss atomistic simulations of dislocation processes in copper based on effective medium theory interatomic potentials. Results on screw dislocation structures and processes are reviewed with particular focus on point defect mobilities and processes involving cross slip. For example, the stability of screw dislocation dipoles is discussed. We show that the presence of jogs will strongly influence cross slip barriers and dipole stability.

We furthermore present some new results on jogged edge dislocations and edge dislocation dipoles. The jogs are found to be extended, and simulations of vacancy controlled climb show the jogs to climb easily in their extended form. The stability of small vacancy dipoles is discussed and it is seen that the introduction of jogs may lead to the formation of Z-type faulted vacancy dipoles.

1. Introduction

The concept of a dislocation was established already in the middle of the 1930s, where the introduction of the edge dislocation in 1934 by Orowan [1], Polanyi [2] and Taylor [3], and the screw dislocation in 1939 by Burgers [4] revolutionized the understanding of crystal plasticity (for a detailed historical introduction to dislocations, see [5]). In spite of the long history, many fundamental aspects of key dislocation processes still remain unanswered.

In deformed metals, the density of dislocations is controlled by two competing processes: the rate of dislocation creation and the rate of annihilation of dislocations with opposite sign. Experimentally, the annihilation of such dislocation dipoles has been investigated intensely, e.g. in fcc metals like copper [6–9] and nickel [10–12]; but essential aspects of the actual nature of the annihilation process for both edge- and screw dislocation dipoles still remained unknown. The primary reason that they eluded discovery was because the length scale of the rate-limiting processes was inaccessible to standard experimental techniques such as transmission electron microscopy (TEM). Theoretical attempts to determine the processes were made, but

the applicability of analytical modelling based on dislocation theory to solve these types of problems is questionable. The processes involve the recombination of dislocation cores, at which an elastic description of dislocations breaks down, rendering results associated with a large degree of uncertainty. Within the last two decades, advances in computational power as well as the development of new algorithms have opened the door for fully three-dimensional (3D) atomic scale simulations of such dislocation processes.

Advances in experimental techniques have revealed new insight about dislocations, especially through the introduction of methods such as scanning tunnelling microscopy (STM) [13], 3D x-ray diffraction microscopy [14], and combined high-resolution electron microscopy (HREM) and image simulation techniques [15]. Many of the recent discoveries, verifications and realizations regarding dislocation activity in the bulk of crystals have, however, also been provided by computer simulations.

Simulations elucidating the role of dislocations for plastic behaviour are complicated by the fact that several different length scales play an important role. The motion of a dislocation involves a shifting of the atoms in the dislocation core and the atomistic structure of the core is therefore of great importance for the dislocations mobility. Also for the nucleation of new dislocations and for the properties of point-like defects such as jogs or kinks, the atomistic details are important. However, the long-ranged elastic interactions between dislocations play a dominant role in the formation of mesoscale dislocation networks, which may control the resulting plastic behaviour of the macroscopic material. Due to the difficulty in treating the multiple length scales, most present day studies of dislocation dynamics focus on only one particular aspect of the dislocation behaviour.

Full electronic structure calculations based on density functional theory (DFT) can be used to study the structure of metal systems of rather limited sizes involving up to, say, a few hundred metal atoms. This has recently been shown to be sufficient to investigate the properties of screw dislocation cores in bcc metals such as Mo and Ta [16, 17]. For fcc metals with a relatively low stacking fault energy, such as copper, the dislocations split into Shockley partial dislocations and a direct study of the extended core structure using DFT becomes difficult. Still, DFT calculations can provide useful information about the core structure through calculations of key quantities such as elastic constants and stacking fault energies. Different core properties can then be obtained by combining such information with dislocation models. This approach has, for example, recently been used to study aluminium dislocation cores using a generalized Peierls–Nabarro model with the generalized stacking fault energy surface calculated with DFT [18, 19].

At the other end of the spectrum, the long-range interactions between separated dislocations are well described using linear elasticity theory and there is no longer a need for an explicit description of the electronic or atomic degrees of freedom. This forms the basis for dislocation dynamics simulations [20–23], where the dynamical objects are the dislocation lines, and all information from the electronic/atomistic level is condensed into a set of rules governing dislocation behaviour at short distances. A recent supplement to these methods are the quasi-continuum models [24, 25], which combine atomistic and elastic calculations in one simulation.

In an intermediate length regime where both the core and the elastic properties of dislocations come into play, a direct self-consistent electronic structure approach is often not possible and one has to resort to more approximate ways of treating the atomic interactions. The challenge here is to find computationally efficient methods, which at the same time retain the relevant electronic information. In most cases this means either the use of tight-binding schemes [26], where the electronic degrees of freedom are still maintained but the description of the Hamiltonian matrix is much simplified or, for even larger systems, e.g. dissociated dislocations in fcc metals, the use of interatomic potentials where there is no direct reference to the electronic states.

In this paper we review results on atomistic simulations of single screw dislocation cross slip in copper, the annihilation of screw dislocation dipoles, and the effect of jogs and kinks on these processes. We also present new results on the structure and climb of jogged edge dislocations, as well as the annihilation of edge dislocation dipoles and the formation of faulted Z-type vacancy dipoles. The simulations have been performed using effective medium theory (EMT) [27–31] based potentials.

2. Simulation issues

The EMT is derived from DFT and the resulting potentials include many-atom interactions through a nonlinear dependence of the energy on the local electron density. The obtained mathematical form of the potentials used here [31] is very close to the one used in other popular metal potentials like the Finnis–Sinclair potential [32, 33] or the embedded atom method [34, 35]. As is common in the construction of interatomic potentials, a small number of parameters are not directly calculated but adjusted to experimental results as described in detail in [31].

It is an important issue whether the interatomic potential reliably describes the energetics of relevant atomic structures. Some insight into this issue can be obtained from the derivation of the potential [27] but otherwise one has to rely on direct tests of the potential on relevant quantities. We shall not go into a more general discussion of the EMT potentials here but will focus on only one particular aspect of high relevance for dislocations, namely the stacking fault energy. The dislocations in fcc metals with a low stacking fault energy are split up into partial dislocations with an intrinsic stacking fault ribbon extending between the partials. The width of the ribbon is determined by a balance between the elastic repulsion of the partials and the energy cost of creating the stacking fault ribbon. The stacking fault energy is therefore of great importance for the dislocation structure and energetics. The stacking fault energy is, however, a rather delicate quantity to calculate: the interatomic distances and number of atoms surrounding an atom positioned at a stacking fault (hcp registry) is the same as in the bulk crystal (fcc registry) for the first two neighbour shells, and the energy difference can be quite small; for the noble metals as low as a few meV per atom. The stacking fault energy is in principle accounted for in the EMT through the so-called one-electron energy term [27], however, this has not been taken into consideration in the earlier practical implementation of the potentials [31]. Getting the stacking fault energy right therefore requires special attention in the construction of the potential.

Stacking fault energies have been calculated using DFT for a wide range of metals [18, 36, 37]. Of particular interest here is a study [36] where a localized LMTO basis set was used in a force-theorem type calculation of stacking fault energies in closed-packed metals. The method allowed for a decomposition of the resulting energies into contributions from the different atomic layers around the stacking faults. Such layer-projected stacking fault energies are shown in figure 1 as solid curves for a range of metals. An analysis [38] of these calculations indicates that for the noble metals Cu, Ag, and Au the energy profiles through the stacking faults can be understood based on simple pairwise interactions between the atoms, while for the other metals the atomic interactions are of a more complicated nature. In the figure this can be seen from the columns, which have been obtained through a fitting of the calculated energies to a model with a sum of pairwise interactions (black columns) and an energy term proportional to the fourth moment of the density of states (white columns) [38]. The pairwise interactions are seen to carry the main responsibility for the (low) stacking fault energy of the noble metals, while a higher order interaction model is necessary to account for the (higher) stacking fault energies of aluminium and the late transition metals. In the latter

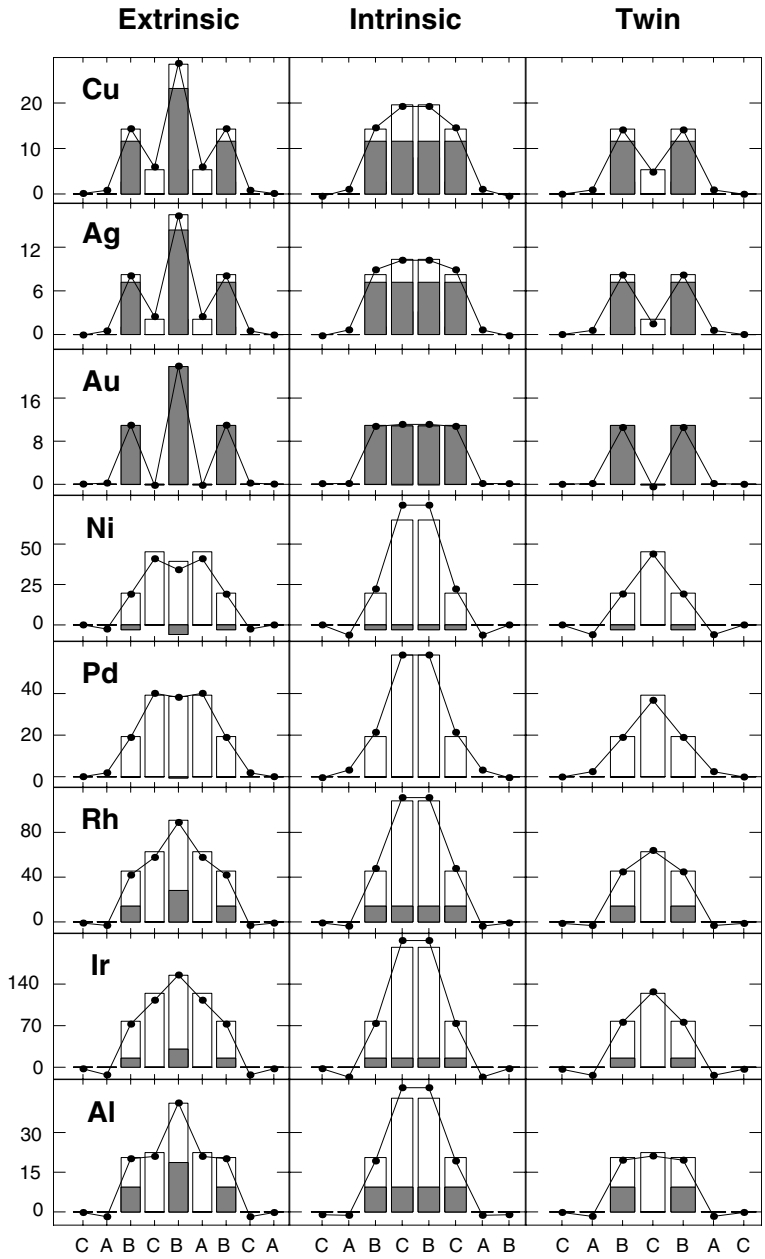

Figure 1. Stacking fault energies. Layer-by-layer energy contributions to the extrinsic, intrinsic, and twin faults. The solid lines are the results of local-density calculations in [36]. The solid part of the bars is the contribution from the pair potential and the open part is the contribution from the fourth moment of the density of states. For the noble metals, Cu, Ag, and Au, the contribution from the pair potential is seen to dominate (from [38], copyright by the American Physical Society).

metals, the partly filled *d*-bands tend to form directional bonding, whereas neither the pure *s*- nor the filled *d*-band in the noble metals contribute to the fourth moment.

The EMT potentials used in the work presented here have had the long-range part (around

the third nearest neighbour shell) of the pair-interaction term adjusted in order to reproduce reasonable stacking fault energies [39,40]. Based on the above-mentioned analysis this seems a reasonable approach for the noble metals. However, already for the late transition metals Ni, Pd and Pt the representation of the stacking fault energy using pairwise interactions becomes questionable.

Several of the dislocation processes we shall consider in the following are thermally activated processes and one of the goals of the simulations is to determine the reaction mechanisms and the corresponding activation energies. The so-called *nudged elastic band* (NEB) technique is a convenient method for identifying reaction mechanisms and locating transition states (i.e. saddle points in the energy landscape) for complicated processes involving many degrees of freedom. The method has been described in detail elsewhere [41–43] and here we therefore only briefly present the main idea. The method presumes that both the initial and the final states of the process are known and a simulation starts out with an initial path connecting the initial and final states in the multidimensional configuration space. This path is then 'relaxed' in the sense that it is moved according to the force on each atomic configuration until the forces perpendicular to the path vanishes. The resulting so-called minimum energy path will go through one or more saddle points connecting the initial and final states. In practice the continuous path is represented in the computer by a discrete set of 'points' along the path, each of these points corresponds to a complete atomic configuration of the entire system during the process. The points are then moved perpendicular to the path in the direction of the force acting on the atomic configuration. The points can be distributed along the path by connecting them with springs which can move the points only along the path [41,42]. The spring constants can be varied along the path to control the distribution of points and increase the resolution around the transition state. Recently, it has also been suggested to let one of the points climb along the path to the saddle point [43].

3. Screw dislocation cross slip

Of the dislocation processes discussed in this paper, one process is of particular importance: cross slip of a screw dislocation. The term 'cross slip' refers to the mechanism by which a dissociated screw dislocation crosses over from its primary slip plane into a secondary slip plane (the cross slip plane). The dissociation of a dislocation in a low stacking fault fcc metal is a strong limiting factor on its mobility effectively restricting its glide to only one plane, making, e.g. the bypassing of obstacles in the plane very difficult. Cross slip has been linked directly to macroscopic phenomena in plastic deformation such as the onset of stage III in the work hardening curves of monotonically deformed single crystals. Furthermore, cross slip is necessary for the annihilation of screw dislocation dipoles, which plays a key role in limiting the dislocation density.

In the 1950s and 1960s three different mechanisms for the thermally activated cross slip process were suggested: the Friedel [44] and Escaig [45] (FE), the Schoeck and Seeger [46], and the Fleischer [47] mechanisms, respectively. Determining which of these mechanisms could best account for the physical process has been hampered by the lack of direct experimental methods to study the process. Treating the problem within the framework of elasticity theory [48, 49] is also difficult because the process involves the overlap of dislocation cores and calculated results are therefore quite sensitive to the choice of dislocation core cut-off [48, 50].

Cross slip of single, straight screw dislocations have been simulated for copper [39,51,52] using an EMT potential and for nickel [53] using an EAM potential. It was found in the atomistic simulations that without any externally applied stresses the process occurs in

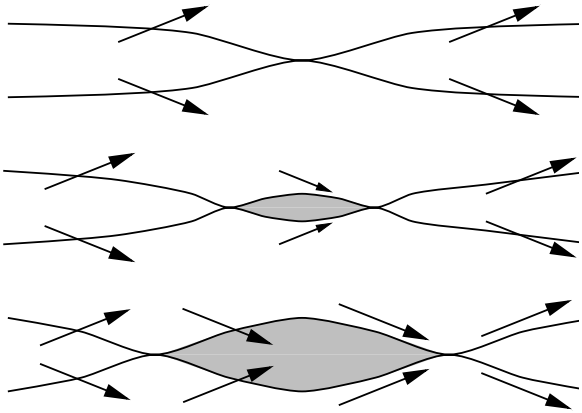

Figure 2. The FE cross slip mechanism. The Burgers vectors of the Shockley partials are indicated with arrows. Cross slip is initiated by the formation of an in-plane Stroh constriction (top), which dissociates into two twisted constrictions thereby taking the dislocation into the shaded cross slip plane (middle). The twisted constrictions move apart (bottom), and complete the transition into the cross slip plane. The twisted constrictions are denoted edge- and screw-like, respectively (from [40]).

accordance with the FE mechanism, see figure 2. In the FE mechanism, the Shockley partial dislocations form a Stroh-type constriction [54] in the primary glide plane (top), which changes into twisted edge- and screw-like constrictions thus initiating the redissociation into the cross slip plane (middle). The constrictions then move apart and complete the process (bottom). The two different types of constrictions formed were also found to have different energies with the peculiar property that the screw-like constriction has *negative* energy [39, 53].

In experiments of screw dislocation cross slip in copper single crystals, Bonneville and Escaig found quantitative agreement with the FE model [55], and later performed the only experiment aimed directly at determining the activation energy of the process, yielding a value of $E_{\mathrm{exp}} = 1.15 \pm 0.37$ eV [56]. Rasmussen *et al* [39] on the other hand, calculated an activation of 2.7 eV using an EMT potential and the NEB path technique. These values appear to be quite incompatible. Barriers calculated with line-tension models range from 1.3 to 3.5 eV [48, 49, 55, 56], depending upon the chosen cutoff and procedure (for details, see [40]).

The experiments by Bonneville *et al* are performed at high levels of sample deformation, and the experimental situation is thus far from the idealized simulational setup of an isolated dislocation cross-slipping. It could therefore be argued that the effect of dislocation–dislocation interactions should be included in the simulations, in order for them to become representative of the experiments. One possibility, which we shall return to later, is that point-like defects like jogs may come into play.

4. Annihilation of screw dislocation dipoles

A dislocation process which is directly related to the cross slip mechanism is the annihilation of screw dislocations of opposite signs. One of the parameters controlling the maximal dislocation density in a metal is the minimum stable screw dislocation dipole height, i.e. the minimum stable distance between two screw dislocations in different glide planes parallel to each other; below this height the dipole annihilates spontaneously.

In TEM images of cyclically deformed copper single crystals, Mughrabi *et al* [6]

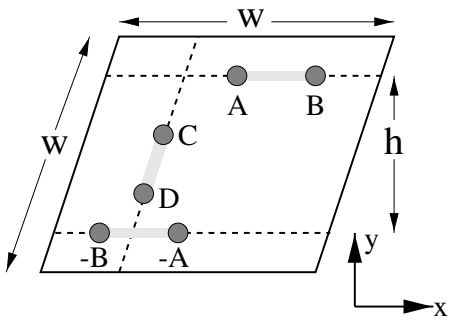

Figure 3. Annihilation of screw dislocation dipoles. Sketch of the geometry of the system setup illustrating the possible dislocation configurations. The two dislocations are parallel to the [110] direction perpendicular to the paper. The dashed lines denote possible glide planes, $(1\bar{1}1)$ (horizontal) and $(\bar{1}11)$ (inclined). The dislocations are depicted as two Shockley partials (dark grey) bounding a ribbon of intrinsic stacking fault (light grey). The partials are A $= \frac{1}{6}[21\bar{1}]$, B $= \frac{1}{6}[121]$, C $= \frac{1}{6}[12\bar{1}]$ and D $= \frac{1}{6}[211]$. CD is to be understood as a cross slipped AB. For a cross slipped $-$ (AB) dislocation, D and C should be replaced by $-$C and $-$D, respectively (from [57]).

investigated the dislocation structure of persistent slip bands. Investigating screw dislocation dipoles, they observed none with heights below 45–50 nm at room temperature. These findings do not exclude the existence of smaller screw dipoles, and the often quoted minimum stable dipole height of 50 nm is therefore to be regarded as an upper bound. On the other hand, no observations of smaller dipoles have to our knowledge been made for copper. In the following we shall see that atomistic simulations indicate that at low temperatures direct spontaneous annihilation of isolated screw dipoles does in fact only happen at much smaller distances.

The annihilation of jog-free screw dislocation dipoles in copper has been simulated using an EMT potential and the NEB technique [57]. Using the computational set-up illustrated in figure 3, the reaction path for the annihilation process could be studied and the corresponding activation energies determined as a function of dislocation separation (the dipole height).

Only screw dislocation dipoles of heights less than 1 nm were seen to be unstable and annihilate spontaneously at low temperatures. For higher dipoles, the dislocations align in a stable, skew equilibrium configuration at an angle close to that of the glide planes (see figure 3); the skew configuration being a result of elastic anisotropy in copper.

The separation of the partial dislocations in each of the screw dislocations depends strongly upon the height of the dipole. This is a result of the stress field from the other dislocation acting upon the edge components of the partials and forcing them together. The shorter the separation, the less energy is required to make one of the dislocations constrict and subsequently initiate cross slip. The exact nature of the cross slip process initiating the annihilation therefore also depends somewhat upon the dipole height, but the mechanism corresponds qualitatively to the FE mechanism (for details see [57]). The second dislocation asserts a strong attractive force on the dislocation loop in the cross slip plane, thereby resulting in a gradual shift of the transition state away from the stress-free FE mechanism, as illustrated in figure 4. The figure shows selected configurations from the obtained annihilation path for a dipole height of 15 $(1\bar{1}1)$ planes, where the cross-slipping dislocation glides over to the other one and completes the annihilation [57].

For dipoles of heights 1–3 nm, the activation energy was found to vary almost linearly with the inverse dipole height (see figure 5). In the limit of high dipoles (low stresses), the barrier approaches the activation energy for cross slip of a single screw dislocation, and the

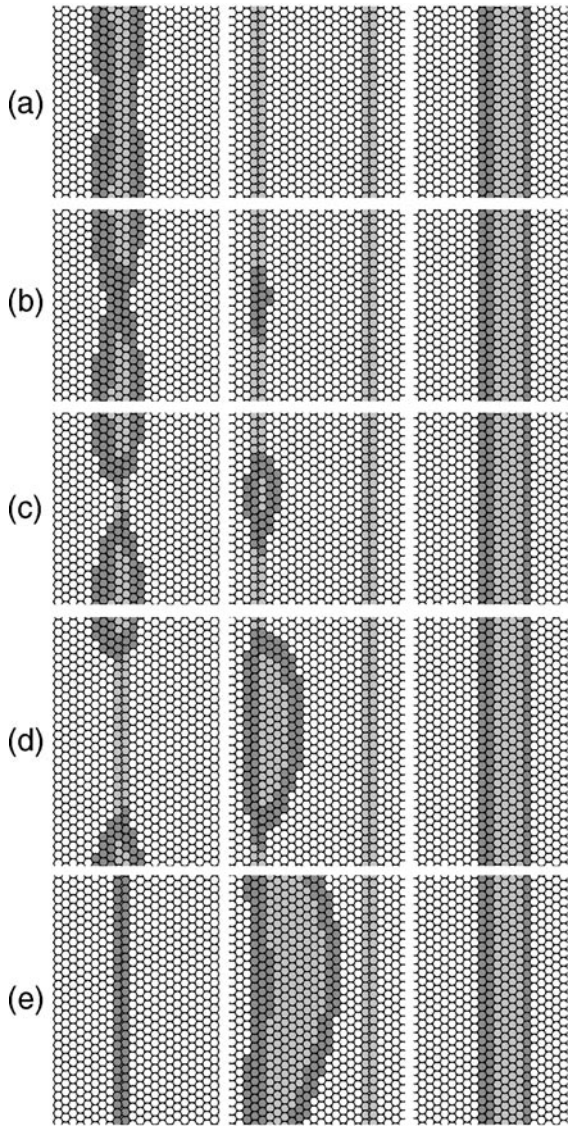

Figure 4. Annihilation details. Details of the cross slip process leading to annihilation for a dipole height of 15 $(1\bar{1}1)$ planes. In each row, the figure shows the initial glide plane for the negative (positive) dislocation in the left (right) column as defined in figure 3; the center column shows the cross-slip plane. The transition state is seen in (c) (from [57]).

point for infinite dipole height is the cross slip activation energy for a single screw dislocation (2.7 eV obtained previously with this potential [39]).

The annihilation simulation also provides some information about the activation volumes of the cross slip process, i.e. the derivatives of the activation energy with respect to the stress. As the height of the dipole is varied, the different stress components exerted by one dislocation in the dipole on the other one change, and the resulting shift in the energy is related to the activation volume for this particular stress combination. The activation volume can be expected to vary significantly in the low stress limit where the twisted constrictions are well separated

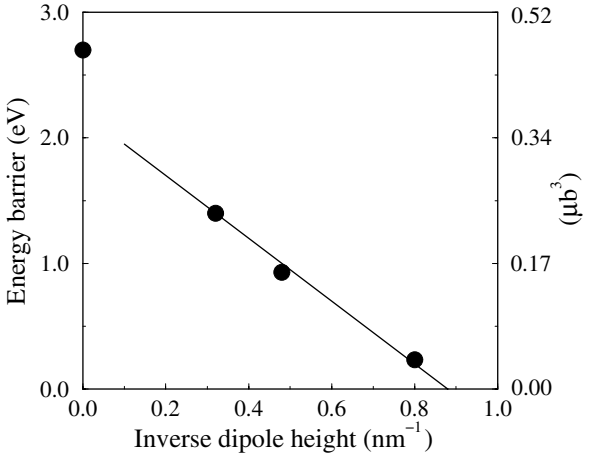

Figure 5. Annihilation energy. The annihilation activation energy as a function of inverse dipole height for jog-free dipoles. The point for infinite dipole height is the cross slip activation energy for a single screw dislocation [51], i.e. not from an annihilation simulation. The slope of the straight line yields the cross slip activation volume (from [57]).

in the transition state. From the figure a typical value of around $\simeq 15b^3$ can be deduced for high stresses present in the 1–3 nm high dipoles. Bonneville *et al* found $\simeq 300b^3$ in their cross slip experiments, but as already alluded to the exact identification of the atomistic process responsible for the process may not be clear.

For dipole heights of the order 50 nm, the activation energy must—from the simulations (see figure 5)—be expected to be in excess of 2 eV. With such a high energy barrier even long dislocation segments would be expected to be stable for very long times at room temperature: the Boltzmann factor is smaller than $\exp(-80) \approx 2 \times 10^{-35}$ and it would require an anomalously high rate prefactor for the annihilation process to occur on an experimental timescale.

The argument above relies on the use of transition state rate theory (TST) [58, 59], where an Arrhenius form for the annihilation rate, r, is obtained:

$$r = \nu \exp(-E/k_B T). \tag{1}$$

Here E is the transition state energy, T the temperature, and ν denotes the rate prefactor. A number of assumptions lie behind the Arrhenius form for the rate and we shall briefly discuss the essential ones. For a more detailed discussion of these aspects the reader is referred to [58, 59].

Consider a process leading from an initial to a final state with a single transition state TS (i.e. a saddle point in the energy surface) located at a so-called dividing surface separating the two states in configuration space. At sufficiently low temperatures the rate is determined by reaction paths passing very close to the TS, and it is possible to consider only the region around the TS in which a harmonic approximation to the potential energy surface is valid. If we furthermore assume that trajectories passing through the dividing surface towards the final state always complete the reaction (neglecting so-called 'dynamical recrossings') the Arrhenius form in equation (1) is obtained, where E is the (zero-temperature) energy of the TS relative to the initial state. The prefactor will have only a weak power-law dependence on the temperature, and the power is determined by the number of available free-translation modes in the initial and transition states. At higher temperatures anharmonic effects can come into play

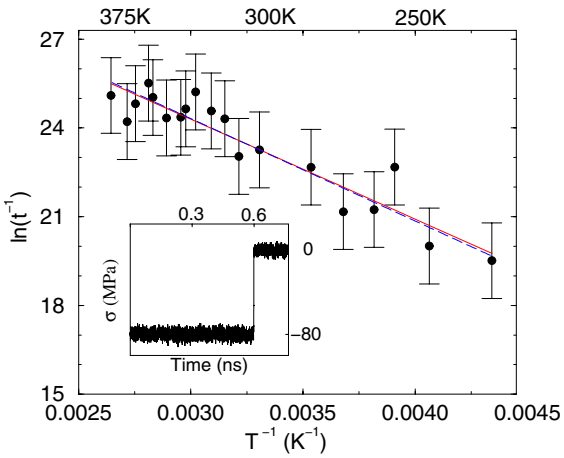

Figure 6. Annihilation rate. An Arrhenius plot of the dipole 'life time' as a function of the simulation temperature. The full line is a linear fit to the life times, yielding an activation energy of 291 ± 27 meV and a ν value of 4×10^{13} s^{-1} b^{-1}. The dashed line is the best fit to the data points for a line with slope corresponding to the zero Kelvin NEB activation energy of 315 meV. This yields a ν value of 5×10^{13} s^{-1} b^{-1}. The insert shows the $\sigma_{[110][1\bar{1}2]}$ component as a function of time for the MD simulation at 255 K used to determine the life time of dipole (from [60], copyright by the American Physical Society).

and also dynamical effects may show up. The activation energy appearing in the exponent in equation (1) can then acquire a temperature dependence, and also the prefactor may change.

Returning to the dipole annihilation, the question is whether the simple harmonic rate theory is applicable or if anharmonic and dynamical effects are so strong that activation energies and prefactors will be significantly changed.

This point has been investigated using direct molecular dynamics simulations of the annihilation of screw dislocation dipoles in copper [60]. In general, the annihilation process cannot be studied with molecular dynamics; due to the high-energy barriers an annihilation would not occur on the timescale of a typical molecular dynamics simulation. Of course, this is the reason to invoke rate theory and to use the NEB technique in the first place. However, for dipoles where the separation between the dislocations is sufficiently small, the barriers become so low that molecular dynamics simulations of the annihilation becomes possible.

Figure 6 shows a comparison between molecular dynamics and rate theory for the annihilation process in copper [60]. A screw dipole with a height of 1.3 nm and a length of the supercell of $30b$ was set up in a similar way as described in section 4. Based on NEB simulations, the transition state energy was determined to be 315 meV. The system was then heated to temperatures in the range between 225 and 375 K using Langevin dynamics [61]; the lower temperature bound was determined by the timescale accessible to the atomistic simulations and the upper bound by annihilation during the sample heating procedure. After the heating procedure, the thermalized system was subjected to Newtonian dynamics (Verlet) until the dislocation annihilation occurred. The time required to obtain annihilation, i.e. the 'life time' of the dipole, could be clearly determined by monitoring the stress components in the simulation (insert in figure 6) since no re-crossings were observed.

A total of 19 MD simulations were performed at various temperatures in the accessible interval. The data are shown in figure 6 in an Arrhenius fashion with the life time versus the inverse temperature. The 'error bars' in the figure come from the assumption of exponentially

distributed life times, t, at a given temperature, since only one simulation was performed at each temperature. It is seen from the figure that the data points can be fitted with a straight line, and a least squares fit leads to the value $E = 291 \pm 27$ meV of the activation energy, which agrees very well with the transition state energy of 315 meV obtained by the NEB simulation.

A rate prefactor of $\nu = 2 \times 10^{15}$ s^{-1} could be determined for this specific dislocation length. Due to the translational symmetry along the dislocation it is, however, more natural to consider the rate prefactor per length of dislocation, which has a typical atomic-scale value of 4×10^{13} s^{-1} b^{-1}.

Modelling the annihilation process with a simple line tension model using harmonic TST, the prefactor can be shown to be proportional to the length of the dislocation and furthermore to depend on temperature as $T^{-1/2}$. The weak temperature dependence was not observable in the narrow temperature range of the simulations, for details see [60].

The simulations indicate that TST is quite applicable also to complicated dislocation processes involving very many atomic degrees of freedom. In the case of the dipole annihilation, the obtained prefactor has a size typical for atomic processes.

5. Jogs and kinks on screw dislocations

Glide of dislocations in their primary glide plane is limited by, among other things, the presence of dislocations on intersecting glide planes. Such *forest dislocations* are present even in well annealed samples. In some situations, the intersection of dislocations by other dislocations will lead to the formation of point-like defects on the dislocations, known as jogs and kinks. A jog is a segment of the dislocation line which has a component of the sense vector normal to the glide plane, whereas a kink is a segment contained within the glide plane. The generated jogs or kinks will be equal in length and direction to the Burgers vector of the intersecting dislocation.

In the following sections, we will review some of the properties of jogs and kinks on screw dislocations in copper as obtained from atomistic simulations. In particular, we shall see that the presence of jogs greatly reduces the energy barrier for cross slip and also affects the stability of dislocation dipoles.

5.1. Jogs

Figure 7 shows the structure of a unit jog with line vector $l = a[001]$ on a $\boldsymbol{b} = \frac{a}{2}[110]$ screw dislocation dissociated in the $(\bar{1}11)$-plane as obtained by atomistic simulations [62]. The jog is seen to greatly influence the dislocation structure by causing the two partials to constrict around the jog. Also a jog with line vector $\frac{a}{2}[101]$ causes the dislocation to constrict; this can be seen in frame (a) of figure 8. The fact that the jogs are constricted is in good agreement with findings of Zhou *et al* [63], who also observe jogs on screw dislocations to be constricted in their simulations on copper.

Because the presence of the jog introduces a constriction of the partials the formation energy for a jog is high, around 2.4 eV for the jog with line vector $\frac{a}{2}[101]$. The number of jogs present due to thermal equilibrium fluctuations, say at room temperature, will therefore be very small. However, jogs can be introduced by the intersection of dislocations out of equilibrium, e.g. during straining of the sample.

The mobility of jogs on both octahedral $\{111\}\langle 110\rangle$ and non-octahedral $\{110\}\langle 110\rangle$ slip systems has been investigated, yielding migration energies of only 15–20 meV for the conservative jog migration along the line of the screw dislocation [62, 64]. This is about an order of magnitude lower than the 'several tenths of an eV' predicted by Hirsch using an elastic description [65]. Although the non-octahedral slip systems are not ordinary slip system in fcc

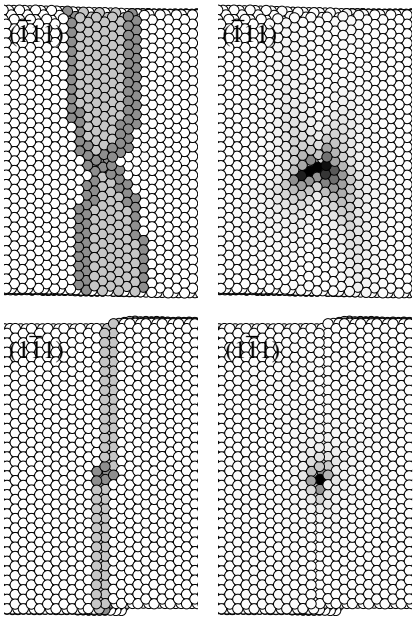

Figure 7. Jog-structure. A dissociated screw dislocation with an elementary jog: $l = a\,[001]$. Top row: the $(\bar{1}11)$ glide plane. Bottom row: the $(1\bar{1}1)$ glide plane. Left column: atoms coloured white are in fcc registry, light grey atoms are hcp, and dark grey atoms belong to the dislocation cores. Right column: the relative scalar atomic displacements associated with a $1\boldsymbol{b}$ jog migration along the dislocation. The darker the colours the larger the displacements (from [62], copyright (2000) by Elsevier Science).

metals, glide has been observed experimentally [66–68], and the calculated barriers are only marginally higher than those for the octahedral slip systems.

Using the effective mass approximation [5], the masses M^* of the jogs can be calculated from

$$M^*(Q) = M_{\mathrm{Cu}} \sum_i (\mathrm{d}q_i/\mathrm{d}Q)^2 \tag{2}$$

where Q is a collective coordinate describing the position of the jog and where the sum runs over all atomic positions q_i; M_{Cu} denotes the mass of a copper atom. If the reaction path calculated with the NEB method is used to determine the collective jog coordinate, the masses for both jogs are found to be rather independent of position and in the range 0.4–0.5 M_{Cu} [62,69]. The distribution of the effective mass, i.e. the separate contributions from the atoms to the sum on the right-hand side of equation (2), is well localized around the jog as can be seen from figure 7. This is in accordance with the fact that the calculated mass is not much smaller than the bare atomic mass.

Because the introduction of a jog on a screw dislocation leads to the formation of a constriction, the presence of a jog could be expected to make it easier for the dislocation to cross slip. This is in fact the case as will be discussed later.

5.2. Kinks

Some of the structural and dynamical properties of elementary kinks in screw dislocations have been studied in recent simulations [64]. The atomistic structure of a kink ($l_{\mathrm{kink}} = \frac{a}{4}[\bar{1}12]$) on

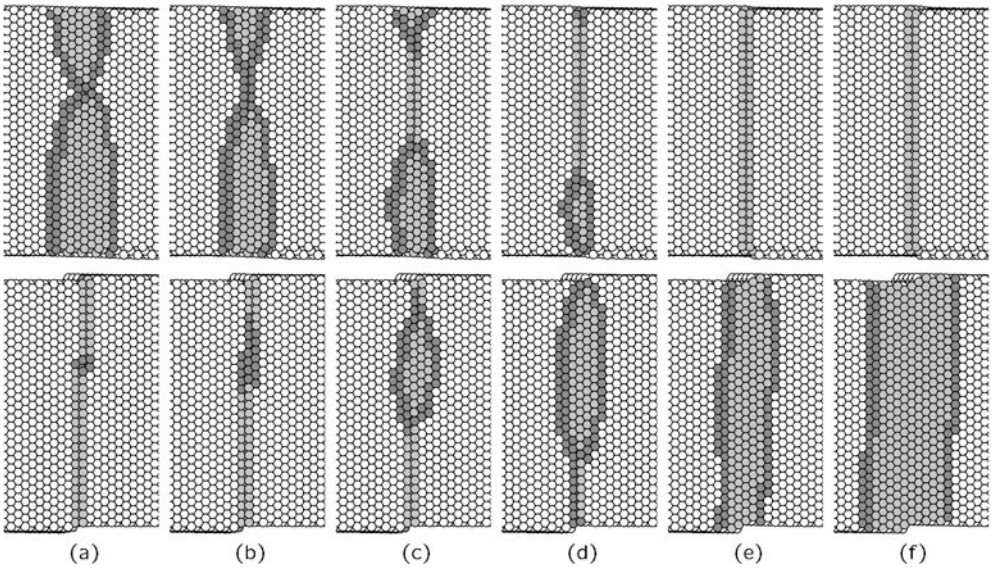

Figure 8. Jogged cross slip. A minimum energy path for the cross-slip of a dissociated $\boldsymbol{b} = \frac{a}{2}[110]$ screw dislocation with an elementary obtuse jog with line vector $l_1 = \frac{a}{2}[101]$. Top row: primary glide plane $(1\bar{1}1)$; bottom row: cross-slip plane $(\bar{1}11)$. The white atoms are fcc atoms, light grey atoms are stacking faults, and the dark grey atoms are in dislocation cores. (a) Initial configuration; (b) redissociation into partial dislocations on the cross-slip plane at the position of the jog; (c) the transition state; (d)–(f) the final transformation into a dissociated, kinked screw dislocation (from [69]).

a dissociated screw dislocation in copper can be seen in part (f) to the right in figure 8. Unlike the jogs, the kink is seen not to lead to any constriction of the dislocation. In fact, the two partials are affected more or less independently each carrying its own partial kink.

Due to the low Peierls barrier in fcc metals, the kinks are very delocalized and spread out, both in the direction along the dislocation line and in the dissociation direction of the dislocation. Elastic calculations have predicted the kinks to be $\leqslant 10b$ wide [70, 71], and the secondary Peierls barrier for kink migration to be as low as $\sim 3 \times 10^{-5}$ eV (0.5 K) [72]. The atomistic simulations confirm that the kink has very peculiar properties. The two partial kinks are both found to be very wide, with a width of around $13b$ for the edge-like partial kink and a width around $21b$ for the screw-like partial kink. The difference in width is a result of the mixed character of the Brugers vectors of the partials, since a kink which forces the dislocation toward the screw orientation will be wider [5].

The energy barrier for migration was estimated by calculating the energy along a linear path in configuration space between the initial, relaxed configuration of a kink and a final configuration obtained by rigidly shifting the kink one Burgers vector along the dislocation line. The total energy of the final configuration is identical to the initial one, due the high precision of the atomic coordinates in the simulation. The resulting upper bound on the energy barrier was found to be only 0.15 μeV. This barrier is about 200 times lower than the above-mentioned elastic estimate made by Schottky [72], but Schottky's estimate was based on a Peierls stress $\sigma_P = 10^{-2}\mu$ and a kink width $w = 10b$. Applying a realistic Peierls stress of $\sigma_P \simeq 5 \times 10^{-6}\mu$ for Cu [73], barriers which are even smaller than the one obtained from the atomistic simulations can be obtained.

The extended kink structure also leads to a very low effective mass for the kink (equation 2). As the kink moves a total distance of 2.5 Å no individual atom moves more than 0.01 Å! Within the straight-line approximation the effective mass was calculated to be only $M_{\mathrm{Cu}}/130$.

The small mass and low barrier of the kink clearly indicates that quantum effects have to be taken into account for the kink motion. In fact, the barrier obtained from the simulations is so low that there is effectively no suppression of quantum tunnelling [64] and even at mK-temperatures the kinks may act as free quantum particles, as suggested in the literature ([5], among others). Growing experimental evidence seems to indicate that atomic tunnelling of defects are involved in quantum creep [74], glassy low-temperature behaviour ([75] and references therein), and low-temperature scaling behaviour in metallic nanodevices [76]. The low mass of kinks certainly make them interesting candidates for quantum behaviour.

6. Cross slip with jogs and kinks

Returning to the jogs, we find that the introduced constrictions on the screw dislocations significantly reduce the barrier for cross slip. Simulations demonstrating this point [62,69] have been performed using a computational setup similar to the one used for the cross slip of jog-free screw dislocations [39, 51]. A screw dislocation with Burgers vector $\boldsymbol{b} = \frac{a}{2}[110]$ was placed in a parallelepiped shaped computational cell with periodic boundaries along the dislocation line. The cell had free surfaces along non-orthogonal, close-packed $(\bar{1}11)$ and $(1\bar{1}1)$ planes; the free surfaces were 79 {111} planes (17.4 nm) wide and the cell was $30\boldsymbol{b}$ (7.6 nm) long, containing approximately 187 000 atoms. The dislocation was dissociated into Shockley partial dislocations on the primary $(1\bar{1}1)$ glide plane: $\frac{a}{2}[110] \rightarrow \frac{a}{6}[121] + \frac{a}{6}[21\bar{1}]$. Jogs were created on the dislocation by changing the periodic boundary conditions of the system, i.e. instead of replicating perfectly along the dislocation line, a small 'mismatch vector' was introduced at the interface between the unit cells; this vector is then the line vector of the introduced jog.

The effect of two different elementary jogs on the cross slip of extended screw dislocations were investigated: (1) $l_1 = \frac{a}{4}[1\bar{1}2]$ is a jog in the $(1\bar{1}1)$ plane and a kink in the $(\bar{1}11)$ plane, see frame (a) in figure 8. The mismatch vector transforms into a lower energy obtuse jog configuration: $\frac{a}{4}[1\bar{1}2] \rightarrow \frac{a}{2}[101] + \frac{a}{4}[\bar{1}\bar{1}0]$ (similar transitions are also seen by Zhou *et al* [63]). (2) $l_2 = a\,[001]$ is symmetrically oriented between the primary and the cross slip plane, and can therefore move conservatively in the $(1\bar{1}0)\,[110]$ non-octahedral slip system.

The cross slip was seen to occur in a very similar fashion for the two jogged configurations. The process occurs in accordance with the FE mechanism, as observed for the jog-free cross slip, except of course for the point that the jog has already caused the formation of a constriction. The redissociation into the cross slip plane is therefore initiated at the position of the jog, where an edge- and a screw-like constriction are seen to carry the dislocation into the cross slip plane. Independent of the line vector of the jog, the activation energy is now only $\simeq$0.9 eV [69].

The calculated barrier for cross slip in the presence of jogs therefore compares much more favourably with the earlier discussed value of 1.15 ± 0.37 eV obtained in the experiments by Bonneville *et al* [56]. A key issue is therefore how large the jog density is in experimental situations like the one described in [56]. These experimental cross slip events take place after activation of a secondary slip system, and jogs are therefore likely formed when the secondary dislocations interact with the forest. The simulations show the jogs to be energetically costly to create but if they are created, by non-equilibrium processes like intersection of dislocations, they can move around quickly over low migration barriers.

7. Dipole annihilation with jogs

The substantial reduction in the cross slip activation energy obtained by the introduction of jogs makes it natural to expect that jogs will also have a strong influence on the annihilation of screw dipoles. This has been investigated [77] in simulations using a similar setup as described for the jog-free screw dipole simulations (see section 4), with two screw dislocations of opposite sign in a unit cell with 3D periodic boundary conditions. The jogs were introduced by changing the boundary conditions as described in the previous section. The obtuse jogs investigated ($l_1 = \frac{a}{4}[1\bar{1}2] \rightarrow \frac{a}{2}[101] + \frac{a}{4}[\bar{1}\bar{1}0]$) are identical to the one in the simulations of a single dislocation (figure 8). This jog was chosen, since it is a kink in the dislocations cross slip plane, and can therefore move conservatively in this plane—effectively without a barrier. The jogged dislocation dipole can hence annihilate without mass transport (i.e. without the activation energies associated with interstitial or vacancy diffusion).

Dipoles with four different heights, $h = n\, d_{111}$ ($n = [4, 6, 10, 15]$) were studied, where the dipole height—describing the separation of the involved glide planes—is measured in units of d_{111} (used henceforth), i.e. the spacing between two adjacent {111} lattice planes. Since the jogs are not introduced in a stable minimum energy configuration, i.e. the atomic positions in the dislocation cores and in particular in the vicinity of the jogs have not been optimized, the dipolar configurations were first relaxed. During this relaxation, the dipoles with heights $h \in [4, 6, 10]\, d_{111}$ annihilated spontaneously, while the $h = 15\, d_{111}$ dipole relaxed to a stable minimum-energy configuration.

It should be noted that with the described setup using 3D periodic boundary conditions, the energy barrier for annihilation can in principle never exceed the barrier for jog-motion along the dislocation lines. If a jog moves along the line a distance, which is equal to the length of the simulation cell, it moves out of the unit cell; but an equivalent jog will have entered the cell at the other end, although shifted by one lattice plane. This will result in a shift of the whole dislocation line by 'l_{jog}' either closer to or away from the other dislocation. If the jogs were free to move they could therefore just continue to move along the dislocations in opposite directions until the two dislocations met and annihilated spontaneously. In fact, the simulations show that below a certain dislocation separation the barrier for jog mobility disappears and the jogs move in this fashion. However, at an even smaller (critical) separation the driving force for direct annihilation via cross slip becomes so large that the annihilation proceeds through this mechanism [77].

Figure 9 shows the reaction path found for a jogged dipole with a height of $h = 15\, d_{111}$. As was observed for the single screw dislocations, the jogs remain constricted (frame (a), figure 9) and can therefore migrate along the dislocation with relative ease. Due to the stress field from the other dislocation, there exists a force driving the jogs in the direction which minimizes the dipole height. The initial migration barrier is only 4 meV (it is 15 meV for an infinitely high dipole) and it diminishes as the dipole height is lowered due to the increased attraction between the dislocations. Below $h = 14\, d_{111}$ the barrier for migration vanishes completely, and the jogs can move freely in this direction. At a certain critical dipole height, $h' = 11\, d_{111}$, one of the dislocations initiates cross slip, see frame (c) in figure 9.

It is thus seen that the presence of jogs significantly affects the stability of screw dipoles. Because of the special setup in the simulations the annihilation can occur via jog migration. However, in reality such a process would require a sufficient supply of jogs, since the dislocations can only move closer by a distance equal to the length of each jog. Jogged screw dipoles below 2.4 nm are seen to annihilate spontaneously via cross slip. Perhaps more importantly, if we apply the values for cross slip of a single jogged screw as the limit of an infinitely high dipole, we can expect barriers associated with the annihilation of a 50 nm

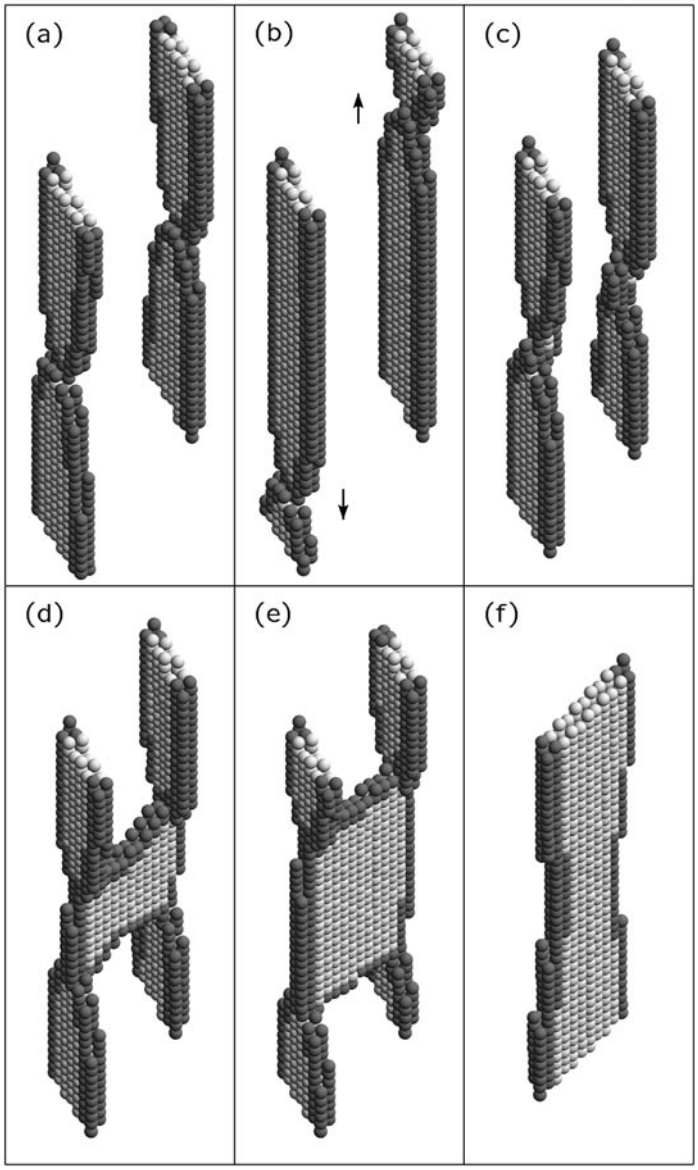

Figure 9. Annihilation of a jogged dipole. The annihilation of a jogged $h = 15(1\bar{1}1)$ planes dipole. (a) The initial configuration. (b) The last meta-stable dipole configuration, as the dipole height is reduced by the motion of the jogs. (c) When $h' = 11(1\bar{1}1)$ planes, the partials A $= \frac{a}{6}[21\bar{1}]$ and B $= \frac{a}{6}[121]$ start to recombine around the jog, and redissociate with partial D $= \frac{a}{6}[211]$ moving into the cross slip plane. (d) The partials $-$A and $-$B then start redissociating, and partial $-$D initiate annihilation with D. (e) The continued jog-motion moves the partial dislocations into the cross slip plane. (f) The remaining partial dislocations C $= \frac{a}{6}[12\bar{1}]$ and $-$C complete the annihilation (from [77]).

screw dipole to be reduced from more than 2 eV to less than 1 eV. With typical atomic rate prefactors, as the one determined for the annihilation of jog-free screw dipoles, such barriers can be overcome at room temperature, and it may be possible to understand the absence of smaller dipoles in the experiments [6].

8. Edge dislocation motion

Having dealt with the properties of screw dislocation annihilation in some detail, we turn our attention to the other predominant factor in limiting the dislocation density: the annihilation of edge dislocation dipoles; in particular, the annihilation of dislocations on two non-intersecting glide planes. This process can only occur via non-conservative motion (including mass transport), i.e. where one of the dislocations moves out of its glide plane—a process known as *climb*.

Based on simple energy considerations, climb of an extended edge dislocation, e.g. in copper, must occur, almost exclusively, via jogs climbing along the dislocation line, while emitting or absorbing either vacancies or interstitials; climb of an entire line defect as a whole is energetically simply too costly [78, 79].

Among other things, climb of edge dislocations has been expected to govern the creep rate in metals, where the minimum creep strain rate is in these cases proportional to the self-diffusion constant [79]. The creep strain rate is proportional to the applied stress raised to a certain power. The exponent in such power law creep expressions is expected to depend heavily on the stacking fault energy, i.e. on the degree of dissociation in dislocations and jogs. Detailed knowledge of the exact atomic nature of such climb processes is therefore essential in trying to determine the activation energies associated with dislocations moving out of their glide planes. Such information is—currently at least—inaccessible to direct experiments on copper, and theoretically only simple hard sphere modelling has been performed for extended edge dislocations with jogs.

Based on hard sphere modelling of an acute unit jog, Argon and Moffatt [79] predicted that climb of an extended dislocation was controlled by vacancy emission from extended jogs—they did, however, argue that atomistic simulations were required. This type of atomistic simulation was recently undertaken by Zhou *et al* who investigated the formation of point-defects by dragging a 60° dislocation with an obtuse jog using an interatomic EAM copper potential. They showed, that under stress, the jog line vector could change from an otherwise conservative orientation to a direction, which caused the formation of vacancies, when the dislocation was dragged; but no activation energies were determined [63, 80].

As discussed in section 5, atomistic simulations on copper have revealed that unit jogs on screw dislocations are constricted [69, 77, 80], whereas jogs on 60° dislocations have been shown to form extended jogs (jog-lines), see [63, 80] for details. In weak beam experiments on the low stacking fault Cu-15.8 at.% Al alloy, Carter [81] have shown that both extended and contracted jogs can exist on the same dislocation line and argued that the level of jog-extension should depend primarily upon the stacking fault energy, the height of the jog, and the orientation of the dislocation line, i.e. the dislocation self-energy. The level of jog-extension is thus expected to be a dominant factor in the energy barriers associated with climb of edge dislocations, see [81] and references therein. Line energy considerations based on the results from jogs on screw and 60° dislocations in pure copper would seem to suggest unit jogs on edge dislocations should adopt an extended configuration, since the self-energy gradually increases from the screw to the edge direction. For superjogs, the elastic calculation made by Hirsch [65], suggesting dissociation of the jogs, must in general be expected to hold, since long jogs will gradually adopt the characteristics of ordinary dislocations.

HVEM on near-edge dislocations in Ag-15 at.% Al have revealed jogs to be extended and shown them to move non-conservatively via the absorption of point-defects [82]—though it is unclear exactly how this climb occurs.

8.1. Migration of point defects

The climb rate of edge dislocations is not necessarily controlled by the energy barriers for the climb of jogs. Due to the required mass transport, the relevant diffusion barriers for

point defects must also be taken into account, see for instance Friedel [78]. The energy required to form an interstitial atom in the bulk of a copper crystal is very high (2.2 ± 0.7 eV in experiments [83] and 2.61 [84] to 3.0–3.2 eV [85] in atomistic simulations), whereas its migration (i.e. the diffusion barrier without including the formation energy) is very easy (0.12 eV in experiments [86] and 0.08–0.10 [85] to 0.11 eV [84] in atomistic simulations). This combination of a high formation energy and a low migration barrier means that few interstitials are formed, and those that are, migrate away easily, e.g. to the surfaces. The diffusion of vacancies is a different scenario; the formation energy is substantially lower (1.31 eV [87] in experiments and 1.26–1.27 [85] to 1.42 eV [84] in atomistic simulations), whereas the migration is much harder (0.70 ± 0.03 [88] to 0.76 eV [87] in experiments and 0.69 [85] to 0.82 eV [84] in atomistic simulations). It is therefore generally believed that it is either the actual climb or some kind of vacancy controlled diffusion/migration, which is rate-limiting for these climb processes.

In the following sections, we will therefore describe simulations of vacancy-controlled climb of jogs, as well as different avenues of vacancy migration such as: pipe migration (i.e. diffusion along the dislocation cores), diffusion along the stacking fault ribbon, and diffusion in the plane of the jog.

8.2. Jog structure

The computational system used to investigate the non-conservative motion of jogs along edge dislocations—and later the annihilation of edge dislocation dipoles, see section 10—contains a vacancy dipole with Burgers vectors $\boldsymbol{b} = \pm\frac{a}{2}[110]$ and line vectors oriented along the $\left[\bar{1}1\bar{2}\right]$ direction. The dipole is placed in a parallelepiped shaped computational cell with 3D periodic boundary conditions. The orthogonal sides of the unit cell are terminated along $\left(\bar{1}11\right)$ and (110) planes, respectively. The sides of the unit cell are 80 $\left(\bar{1}11\right)$ and 50 (110) planes wide and the computational cell is 50 $\left(\bar{1}1\bar{1}\right)$ planes high. The unit cell contains approximately 200 000 atoms—depending on the exact height of the vacancy dipole.

The dislocation dipole is introduced into the cell as a 'stepped' vacancy band, i.e. part of a (110) plane has been removed, and a unit step (jog) is introduced at the interface between the simulational cells in the direction of the dislocation lines. The jogs are introduced in the same manner as described for the screw dislocation dipoles. The applied mismatch vector $l = \frac{a}{2}\left[\bar{1}01\right]$, is in essence a unitary segment of a 60° dislocation. Such jogs could have been formed in a real crystal by a $\boldsymbol{b} = \frac{a}{2}\left[\bar{1}01\right]$ dislocation intersecting the dipole, as illustrated in principle by Zhou *et al* [63].

The vacancy band is then relaxed using the MDmin algorithm [61], into a vacancy dipole consisting of two dislocations each dissociated into Shockley partials in their individual $(\bar{1}11)$ glide planes: $\frac{a}{2}[110] \rightarrow \frac{a}{6}[211] + \frac{a}{6}[12\bar{1}]$ and $\frac{a}{2}[\bar{1}\bar{1}0] \rightarrow \frac{a}{6}[\bar{2}\bar{1}1] + \frac{a}{6}[\bar{1}\bar{2}1]$. In addition, the dislocations have acute, elementary jogs with line vector $l = \frac{a}{2}\left[\bar{1}01\right]$.

The length of the vacancy band (the height of the dipole, h) is varied from 2 to 17 d_{111}. In this way we cover the range from very small dipoles to essentially non-interacting dislocations. For vacancy bands higher than $h = 9\ d_{111}$, the structure with the vacancy band is unstable and automatically collapses into a jogged dipole during an energy minimization. For smaller dipoles, the vacancy band is stable and the system can be heated using Langevin dynamics [61] prior to the energy minimization, in order to obtain the dipolar configuration.

After an energy minimization, the jogs are observed to adopt an extended configuration as shown in figure 10. The partial dislocations are observed to constrict slightly on either side of the jog, but more pronounced is the asymmetry of the constriction process itself. This

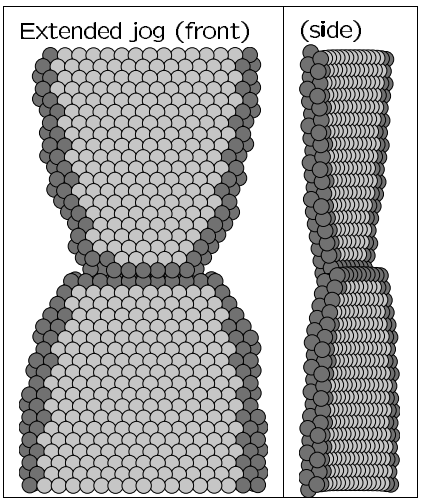

Figure 10. Extended jog structure. The formation of a jog-line ($l = \frac{a}{2}[\bar{1}01]$) is observed on the $\boldsymbol{b} = \frac{a}{2}[1\bar{1}0]$ dislocation (the $[\bar{1}1\bar{2}]$ direction is up) and the constriction of the partials is seen to be very different on either side of jog, due to the orientation of the partials. In the side view (right), the $[1\bar{1}0]$ direction is out of the paper.

asymmetry, i.e. that the dissociation width of the partials is larger on one side of the jog than the other (see figure 10), can be explained by applying simple energy considerations. Due to the mixed character of the partial dislocations, they will tend to align themselves more towards the energetically favourable screw orientation. On the 'narrow side' of the jog the partials are close to the screw orientation and tend to remain so, whereas the energetically expensive edge-like segments on the other side are as short as possible—in fact creating a wider staking fault ribbon in the process. Such asymmetric constrictions around jogs have been observed both experimentally [81,89] and in the simulations of unit jogs on screw dislocations presented here.

The extended configuration is in qualitative agreement with the hard sphere model proposed by Argon and Moffatt, but the asymmetry is naturally not observed in their simple model [79]. Hence, jogs on both edge and 60° dislocations are observed in simulations to be extended, whereas the elementary jogs on screw dislocations are constricted in copper—as also expected from line-energy considerations.

8.3. Climb of an extended edge dislocation

In this section, we investigate the climb of extended jogs. More specifically, climb of an acute $l = \frac{a}{2}[\bar{1}01]$ unit jog on a $\boldsymbol{b} = \frac{a}{2}[1\bar{1}0]$ edge dislocation via the absorption of a vacancy. The process is investigated by applying the NEB method to determine the energetics of the transition from a vacancy in a stable configuration close to the jog (see (a) in figure 11), to the stable configuration, where the jog has absorbed the vacancy and moved one atomic distance in the $[\bar{1}1\bar{2}]$ direction (frame (f)).

The non-conservative jog motion can occur via the emission or absorption of either interstitials or vacancies, but we have focused on the vacancy-dependent climb processes, due to the high formation and low migration barriers for interstitials—as discussed earlier. We have investigated climb by vacancy absorption, with the vacancy placed in different initial positions. We have looked at vacancies placed at the core of either of the $\frac{a}{6}[\bar{2}1\bar{1}]$ and $\frac{a}{6}[\bar{1}2]1]$

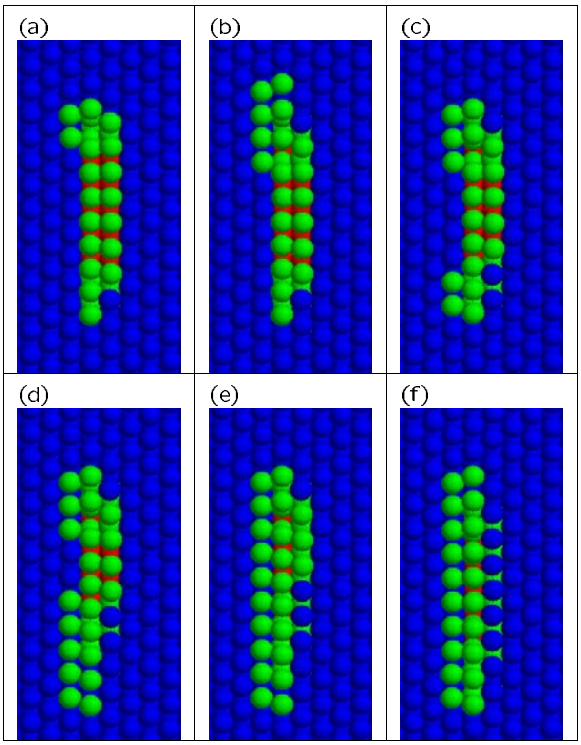

Figure 11. Climb of extended jogs. (colour) Climb of an extended jog via vacancy absorption. In the plane of the jog, with the $[1\bar{1}1]$ normal to the paper, blue atoms are in fcc registry, red atoms in hcp and green atoms are associated with the core of the jog or the dislocations. (a) The initial configuration; (b) gradual absorption of the vacancy; (c) opening at both partials; (d) gradual down-shift of the upper part of the jog-line; (e) the transition state; (f) completing the absorption. The barrier is determined to be less than 0.2 eV.

partials and close to the stacking fault ribbon, in the $(\bar{1}1\bar{1})$ plane of the jog. We have also looked at vacancies near the partials in the adjacent $(\bar{1}1\bar{1})$ planes.

The computational setup applied in these simulations, i.e. the jogged dipole configuration with periodic boundary conditions, introduces a bias in the climb direction. By moving, e.g. the jog on the $\boldsymbol{b} = \frac{a}{2}\left[\overline{1}10\right]$ dislocation in the $[\bar{1}1\bar{2}]$ direction, the average dipole height—and thereby the total energy of the system—is reduced slightly, and *vice versa* for the other direction (or jog).

In all the investigated configurations, we find that the jogs climb by absorbing the vacancy without first forming a constriction. Low activation energies are found for vacancies in the plane of the jog and positioned within one lattice distance from one of the partials. The lowest barrier is found in the compressive stress fields of the partial dislocations; snapshots from such a NEB-simulation are shown in figure 11.

During the absorption, a gradual opening of the jog-line is observed as the upper part of the line shifts downwards (frames (b)). This 'opening' of the jog-line, i.e. the creation of partial vacancies, initiates at the core of both partial dislocations, not only at the core where the vacancy is gradually being absorbed (frame (c)). Finally, the partial vacancies disappear as the jog-line moves down one atomic distance and the atoms redistribute equidistantly in the much wider upper part of the jog-line, until the transition state (frame (e)) is reached. The barrier for

the illustrated vacancy-absorption controlled climb is found be less than 0.2 eV (equivalently low barriers are also observed for absorption at the other partial dislocation). This value is substantially lower than the barriers we find for diffusion from a nearest-neighbour site to the last stable position at the dislocation core (see next section)—the climbing barrier itself is therefore not going to be rate-limiting.

The results are in good agreement with the hard-sphere results, where the acute unit jogs were also found to climb via the creation of partial vacancies, although the hard-sphere model accommodates neither compression nor tension [79].

8.4. Vacancy capture field

Due to the low barriers associated with the constriction-free climb process, it is very likely that diffusion barriers connected with the flux of vacancies will be rate-liming for the climb of jogged edge dislocations in, e.g. heavily deformed copper, where dense dislocation networks can act as effective sinks and sources for point defects [9]. We have therefore also investigated the long-range effects of the presence of extended jogs on the in-plane vacancy diffusion, since any long-range reduction in these barriers could become paramount for the flux in vacancy-rich samples.

We find that only vacancies which are within two atomic distances of either of the dislocation cores or the jog-line have migration barriers significantly lower (by more than 50 meV) than in the bulk. The in-plane extension of this vacancy 'capture field' will therefore only encompass less than 50 atoms, see (a) in figure 11. For such in-plane diffusion to result in an overall lowering of the rate-limiting barrier, the vacancy concentrations must be in excess of several per cent—otherwise the ordinary bulk behaviour will dominate. Other avenues of diffusion related to the presence of the dislocation lines, e.g. core- and ribbon-migration, are therefore more likely candidates for a possible fast vacancy route.

9. Vacancy migration

It is well known that the rate of mass transport is substantially increased in regions of low atomic coordination, e.g. at surfaces [90, 91] and in grain boundaries [92, 93]. The diffusivity can be increased by several orders of magnitude as compared with the bulk [94]. With regards to dislocations, it is generally believed that fast diffusion is especially linked to pipe diffusion, i.e. diffusion inside a $r \simeq 5$ Å cylinder around the dislocation core; the experimental verification of this effect is, however, sparse, see for instance Balluffi [95].

Atomic simulations of diffusion near the cores of extended jog-free edge dislocations have been performed for copper by Huang *et al* [84, 96] using a quasi-two-dimensional procedure, and again recently for aluminium by Hoagland *et al* using an EAM potential and kinetic Monte Carlo methods [97], and by Fang and Wang using a glue-potential [98] in hyper-MD simulations [99]. By calculating jump frequencies of vacancies and interstitials at different temperatures close to the melting temperature, Huang *et al* calculated pipe-migration barriers for vacancies of $E_m^v = 0.77$ eV and for interstitials of $E_m^i = 0.13$ eV [84] using an Arrhenius relation. These values for copper are not significantly lower than those found in the bulk ($E_m^{\mathrm{bulk}(v)} = 0.82$ eV and $E_m^{\mathrm{bulk}(i)} = 0.11$ eV), but for aluminium, both Hoagland *et al* [97] and Fang and Wang [99], have calculated barriers for pipe migration significantly lower than that of bulk.

9.1. Bulk migration

As mentioned, the experimentally determined barrier for migration of vacancies in bulk copper is 0.70 ± 0.03 [88] to 0.76 eV [87]. These values compare reasonably well with the 0.82 eV calculated by Huang *et al* and the 0.69 eV found by Mishin *et al* [85] performing EAM based NEB calculations. Equivalently, Young has experimentally determined the barrier to be 0.12 eV for interstitial diffusion in bulk [86], as compared with 0.11 eV from the atomistic simulations by Huang *et al* [84] and 0.08–0.10 eV by Mishin *et al* [85].

It does therefore seem that interatomic potentials are well suited to deal with these types of diffusion problems in copper. The effect of the electronic contributions, which are not representable by pair potentials, are likely to be small compared with the long-range elastic part of the barrier. In the case of aluminium, recent *ab initio* simulations by Carling *et al* [100] have, however, shown that even DFT calculations have problems describing vacancies, due to electron correlation effects near electronic edges. That the interatomic potentials tend to do better for Cu than Al is, to a large extent, due the tendency in Al to form directional bonds. Encouraging results for interatomic Cu-potentials were also seen by Mishin *et al* [85] who compared values for non-equilibrium structures in copper with *ab initio* and tight-binding results.

With this EMT potential we find an activation energy for bulk migration of a vacancy of 0.79 eV in a fully 3D calculation. We note that long-range elastic contributions play a significant part in this value. Performing the calculation on a unit cell with 47 dynamic atoms (in a $4 \times 4 \times 3$ configuration) surrounded by static atoms, we find that the value is overestimated by $\simeq$0.1 eV [101]. The system size required to include such contributions would render traditional DFT supercell calculation extremely difficult to perform.

9.2. Diffusion along the stacking fault ribbon

Diffusion along the stacking fault ribbon has been suggested as a possible route for fast migration [84, 102], although the atomic coordination (packing) is the same as in the bulk. It should be noted that the conclusions drawn from the experiments [102] were questioned by Balluffi and Granato [103].

Here, NEB simulations have been performed for vacancy migration in a 80 $(\bar{1}11)$ by 60 (110) planes wide and 14 $(1\bar{1}1)$ planes high unit cell. The barrier for vacancy migration in the center of the stacking fault band is found to be 0.74 eV (figure 12), i.e. not significantly lower than the bulk barrier. The simulations by Huang *et al* [84] were performed at temperatures near the melting temperature. At such elevated temperatures, the core of the partial dislocations widens and the traditional perception of the 'core-region' is no longer fully representative. In a metal like copper, where the dissociation width of an edge dislocation is only a few nm, the core region at such temperatures effectively encompasses a large part of the stacking fault ribbon—as the authors also later pointed out [104]. Fast migration in a perfect hcp stacking (the center of the stacking fault band) is therefore unlikely.

9.3. Pipe migration

In our investigations of vacancy migration near the partial cores, we have focused on the barriers for migration along the core of the partials, since this is the relevant direction for vacancy flux required in the investigated climb process.

We find that migration in regions near the partial cores occurs easier than in the bulk; the barriers can be as low as 0.52 eV. The reduction is seen to be slightly more pronounced in the compressive (0.52 eV) than in the tensile (0.53 eV) region, but substantially lower than for bulk in both cases, see figure 12. In the core, the lowest migration barriers are found in the $[\bar{1}0\bar{1}]$ and

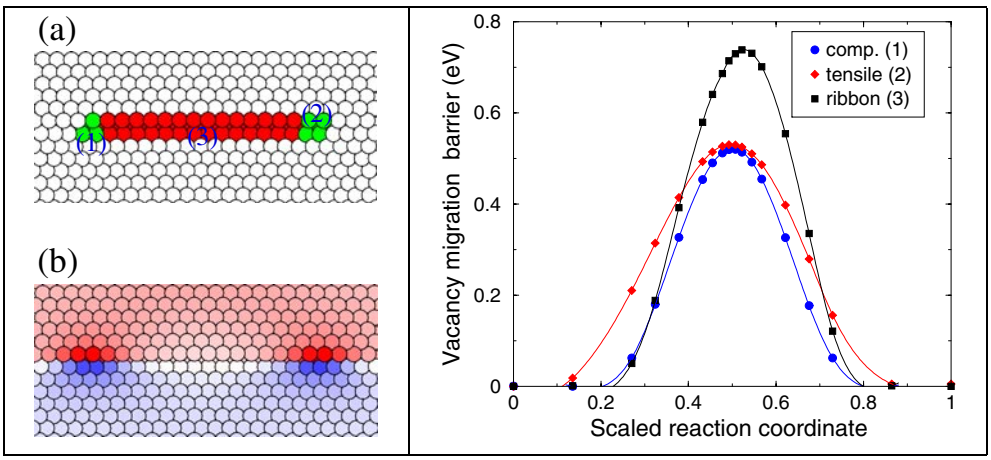

Figure 12. Pipe migration. (colour) (a) The atomic configuration; (b) the stress field, where red corresponds to tensile and blue to compressive stresses; right: the barriers for pipe migration barriers in the compressive (1) and tensile (2) regions around the partial dislocation cores, as well as in the stacking fault ribbon (3).

$[01\bar{1}]$ directions. The vacancies can therefore migrate in the $[\bar{1}1\bar{2}]$ direction by zig-zagging up along the dislocation line in the $[\bar{1}0\bar{1}]$ and $[01\bar{1}]$ directions, respectively. Similar zig-zag paths were found in the core of an aluminium edge partial by Hoagland *et al* [97].

In highly deformed materials, where dense dislocation networks can act as effective sinks and sources for point defects [9], this zig-zag migration in the compressive regions of the core is therefore the fastest way to transport vacancies to and from the jogs. Hence, this process is expected to be rate-limiting for climb under such conditions; at least the low energy barrier points in this direction. However, one should always be careful in interpreting complex phenomena in terms of a single atomistic process. The dominant mobility process in aluminium grain boundaries has, for instance, been shown to depend on the temperature. At high temperatures, the mobility of the low-angle grain boundaries exceeds the mobility of the high-angle boundaries, since the low-angle process not only has the highest barrier, but also the highest prefactor [105].

In situations where the vacancy concentration is low, and the vacancy formation must be taken into account, the compressive region in the core is also where the lowest formation energies would be expected [97].

10. Annihilation of edge dislocation dipoles

The annihilation of two edge dislocations with opposite Burgers vectors requires the transport of either vacancies or interstitials, since one of the dislocations must climb out of its glide plane in order to complete the annihilation. These processes are under normal circumstances thermally activated, and strong attractive forces are necessary to overcome the climb force in order for the annihilation to occur spontaneously.

Based on TEM investigations of persistent slip bands in cyclically deformed copper single crystals, Essmann and Rapp concluded that no edge dipoles below a critical separation distance of $y_c = 1.6$ nm would exist at 77 K [106]. Basinski *et al* [107] later performed experiments on copper at 4.2 K, which furthermore seemed to indicate that the critical annihilation was only weakly temperature dependent and might occur athermally below the critical separation.

The stability of small edge dipoles in fcc metals has recently received much attention, which to a large extent is due to new low-temperature experiments on nickel by Tippelt *et al* [10–12] and on copper by Niewczas *et al* at 4.2 K [8, 9]. Tippelt *et al* find a critical distance in nickel which, although not completely temperature independent, agrees well with the value for copper determined by Essmann *et al*. These findings have led to the surprising suggestion that such a critical separation distance might be independent of both temperature and material [108, 109].

10.1. Jog-free vacancy dipoles

A simple estimate of the stability of (jog-free) edge dipoles can be obtained by comparing the elastic attraction between the dislocations with the force necessary to create, say vacancies, as the dislocations approach each other [78, 108]. This results in a critical dipole height d_c:

$$d_c \leqslant \frac{\mu b^4}{2^{3/2}\pi(1-\nu)E_v^f} \tag{3}$$

where E_v^f is the formation energy of a vacancy. In the case of copper, this critical distance is around 0.4 nm, which is about a factor of four smaller than the above quoted experimental value.

Atomic-scale simulations of the annihilation of edge dipoles in copper and aluminium have been carried out in two dimensions [108, 110]. Aslanides and Pontikis [108] found vacancy edge dipoles in copper to remain stable down to 0.42 nm, whereas vacancy dipoles in aluminium had a critical separation of 1.6 nm [108]. Below the critical values the dipoles were unstable and recombined to form bands of vacancies.

We have performed similar simulations with the EMT potentials for copper essentially confirming some of the results of [108, 110]. Comparing a dislocation dipole structure of height h with a one-atom thick band of vacancies of width h, we find that for $h > 9\,d_{111}$ only the dislocation dipole structure is stable, and the vacancy band spontaneously decays into the dipole structure. In the regime $h = 3$–$9\,d_{111}$ both of the structures are metastable, however, with the dislocation dipole of significantly lower energy. For $h = 2\,d_{111}$ the vacancy structure is most stable, but we also find a stable dipolar structure with almost the same energy (within 5 meV per atomic layer in difference). Finally for $h = d_{111}$ only the vacancy structure (which now consists of a single row of vacancies) is stable. So in conclusion, we find the dislocation dipole to be unstable for $h \leqslant 2\,d_{111}$ which corresponds to a height of 0.4 nm as also found by Aslanides and Pontikis [108].

One may speculate whether the simple, idealized dipolar structures considered above are the relevant configurations for comparison with experiments like those in [106, 107]. The high level of sample deformation, due to strain or sample irradiation in the experiments, may result in the creation of jogs, which can assist in the annihilation procedure. In the following, we therefore present results on edge dislocation dipoles in the presence of jogs.

10.2. Jogged vacancy dipoles

It is well known that long dipoles are intersected by secondary dislocations during, e.g. cyclic deformation, resulting in the formation of shorter, jogged dipoles [111, 112]. Niewczas *et al* [8, 9] have—based on TEM weak-beam diffraction observation and resistivity measurements of copper single crystals deformed at 4.2 K—recently suggested that it is these types of dipoles, which are responsible for the recoverable component of the electrical resistivity. They suggest that such vacancy dipoles could annihilate out during heating to room temperature via a process like pipe diffusion. Such a mechanism could also explain the lack of small dipoles in the images analysed by Tippelt *et al* [10–12] and by Essmann *et al* [7, 106].

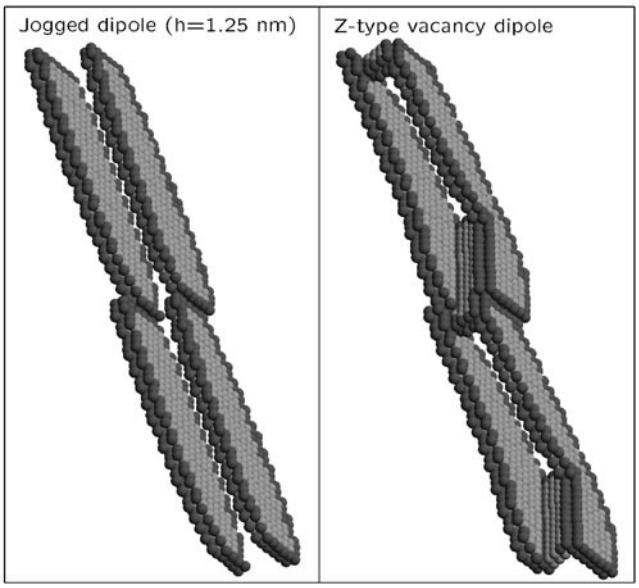

Figure 13. Faulted dipoles. The formation of faulted Z-type vacancy dipole for small dipole heights. A general zig-zagging in the line vectors is observed. The Z-type area depends upon the dipole height and the jog spacing.

The possibilities for pipe diffusion were already discussed in section 9 and here we shall focus only on the structural stability of small edge dipoles with jogs in copper. We have introduced jogs on edge dipoles with heights $h = 1$–$6\ d_{111}$ using the same approach as described for the single edge dislocations.

We find that the simple introduction of jogs on the narrow dipoles, does not result in a general structural instability, which could account for an athermal annihilation mechanism. That is, for heights $h \geqslant 3\ d_{111}$ a stable dislocation dipole structure is obtained. However, we do in some cases observe the creation of faulted Z-type vacancy dipoles [5, 113] on specific areas of the dipole, where jogs are present, see figure 13.

These Z-type vacancy dipole configurations are formed by a transformation of the $C\beta = \frac{a}{6}[\overline{1}\overline{2}1]$ and $\beta C = \frac{a}{6}[12\overline{1}]$ partials:

$$\begin{aligned} &\text{1st disl.: } \frac{a}{2}[\overline{1}\overline{1}0] \rightarrow \frac{a}{6}[\overline{1}\overline{2}1] + \frac{a}{6}[\overline{2}\overline{1}\overline{1}] \rightarrow \frac{a}{6}[\overline{1}\overline{1}2] + \frac{a}{6}[0\overline{1}\overline{1}] + \frac{a}{6}[\overline{2}\overline{1}\overline{1}] \\ &\text{2nd disl.: } \frac{a}{2}[110] \rightarrow \frac{a}{6}[12\overline{1}] + \frac{a}{6}[211] \rightarrow \frac{a}{6}[11\overline{2}] + \frac{a}{6}[011] + \frac{a}{6}[211] \end{aligned} \tag{4}$$

and subsequent annihilation of the two new partial dislocations $C\delta = \frac{a}{6}[\overline{1}\overline{1}2]$ and $\delta C = \frac{a}{6}[11\overline{2}]$, which are glissile in the δ, i.e. the (111), glide plane, leaving behind an intrinsic stacking fault ribbon.

The formation of Z-type dipoles has also been observed experimentally using weak-beam TEM, both for cyclically deformed copper [114] and in Cu-5, 10 and 15 at.% Al alloys deformed in tension [115, 116]. Wintner and Karnthaler have speculated that such faulted dipoles could be formed by either forest cutting or surface nucleated cross slip [116]. All the experimentally observed faulted vacancy dipoles consist of only partial edge dislocations, and we find that the line vectors of the remaining partials in the faulted region align themselves along the $[01\overline{1}]$ edge direction, resulting in the pronounced zig-zagging of the line vectors seen in figure 13.

The extension of the Z-type areas was found to depend on the concentration of jogs (the average jog spacing), as well as the height of the dipole. The lattice distortion produced by such dipoles is of short range (even shorter than for the un-faulted dipoles) and can therefore not be analysed using strong beam diffraction conditions, see Niewczas *et al* [9]. Similar Z-shaped dipolar structures have, however, recently been observed with atomic resolution in GaAs using HREM [117, 118], and the observed zig-zag shape of the dipole agrees well with the one suggested by Tichy and Essmann [110] (and references therein).

Details on the exact conditions under which Z-type vacancy dipoles are formed in the atomistic simulations, as well as the variation of the structure with, e.g. jog density, is currently under investigation.

11. Concluding remarks

Even though dislocations have been known for a long time to lie at the heart of plastic behaviour in metals, the exact role they play for many phenomena in plastic deformation is still not well understood. This situation may be partly caused by the shear complexity of the phenomena under consideration, but one also has to recognize that even at the most fundamental atomic scale, many aspects of dislocation behaviour are still not known. Electronic structure methods and atomistic simulations can in this context provide valuable information about key processes like cross slip or climb—information which may be very difficult to directly obtain experimentally. The reliability of the computational methods is, of course, always a concern and there is certainly a need for improvement both within approximations to the exchange-correlation energy in DFT and in the construction of interatomic potentials. However, the computational techniques have already reached a stage, where they can be used to confront the interpretation of macroscopic experimental results and point to new possible explanations at the atomic scale.

Acknowledgments

The authors would like to thank Torben Leffers, Ole B Pedersen and Torben Rasmussen for inspiring collaboration on dislocation properties, and Jakob Schiøtz and Jens Jørgen Mortensen for valuable comments and insights. The Center for Atomic-scale Materials Physics (CAMP) is sponsored by the Danish National Research Foundation. This work was in part financed by The Danish Research Agency through grants #9501775, #5020-00-0012, and the Engineering Science Centre for Structural Characterization and Modelling of Materials at the Materials Research Department, Risø.

References

[1] Orowan E 1934 *Z. Phys.* **89** 634
[2] Polanyi M 1934 *Z. Phys.* **89** 660
[3] Taylor G I 1934 *Proc. Phys. Soc.* A **145** 362
Taylor G I 1934 *Proc. Phys. Soc.* A **145** 388
[4] Burgers J M 1939 *Proc. K. Ned. Akad. Wet.* **42** 293
Burgers J M 1939 *Proc. K. Ned. Akad. Wet.* **42** 378
[5] Hirth J P and Lothe J 1992 *Theory of Dislocations* 2nd edn (Malabar, FL: Krieger)
[6] Mughrabi H, Ackermann F and Herz K 1979 *Special Technical Publication 675: Fatigue Mechanisms* ed J T Fong (Philadelphia: American Society for Testing and Materials) p 69
[7] Essmann U and Mughrabi H 1979 *Phil. Mag.* A **40** 731
[8] Niewczas M, Basinski Z S, Basinski S J and Embury J D 2001 *Phil. Mag.* A **81** 1121
[9] Niewczas M, Basinski Z S and Embury J D 2001 *Phil. Mag.* A **81** 1143
[10] Tippelt B, Bretschneider J and Holste C 1996 *Phil. Mag. Lett.* **74** 161
[11] Tippelt B, Bretschneider J and Hähner P 1997 *Phys. Status Solidi* a **163** 11

[12] Hähner P, Tippelt B and Holste C 1998 *Acta. Mater.* **46** 5073
[13] de la Figuera J *et al* 2001 *Phys. Rev.* B **63** 165431
[14] Margulies L, Wither G and Poulsen H F 2001 *Science* **291** 2392
[15] Balk T J and Hemker K J 2001 *Phil. Mag.* A **81** 1507
[16] Ismail-Beigi S and Arias T A 2000 *Phys. Rev. Lett.* **84** 1499
[17] Woodward C and Rao S I 2001 *Phil. Mag.* A **81** 1305
[18] Hartford J, von Sydow B, Wahnström G and Lundqvist B I 1998 *Phys. Rev.* B **58** 2487
[19] Lu G, Kioussis N, Bulatov V V and Kaxiras E 2000 *Phys. Rev.* B **62** 3099
[20] Devincre B 1995 *Computer Simulation in Materials Scince. Nano/Meso/Macroscopic Space and Time Scales* ed H O Kirchner, L P Kubin and V Pontikis (Dordrecht: Kluwer)
[21] Devincre B and Kubin L P 1997 *Mater. Sci. Eng.* A **234** 8 and references therein
[22] Bulatov V *et al* 1998 *Nature* **391** 669
[23] Shenoy V B, Kukta R V and Phillips R 2000 *Phys. Rev. Lett.* **84** 1491
[24] Shenoy V B *et al* 1998 *Phys. Rev. Lett.* **80** 742
[25] Rodney D and Phillips R 1999 *Phys. Rev. Lett.* **82** 1704
[26] Turchi P E A, Gonis A and Colombo L (ed) 1998 *Tight-Binding Approach to Computational Materials Science* (*Mater. Res. Soc. Symp. Proc. vol 491)* (Warrendale, PA: Minerals, Metals and Materials Society)
[27] Jacobsen K W, Nørskov J K and Puska M J 1987 *Phys. Rev.* B **35** 7423
[28] Jacobsen K W 1988 *Comments Condens. Matter Phys.* **14** 129
[29] Chetty N, Jakobsen K W and Nørskov J K 1991 *J. Phys.: Condens. Matter* **3** 5437
[30] Nørskov J K, Jakobsen K W, Stoltze P and Hansen L B 1993 *Surf. Sci.* **283** 277
[31] Jacobsen K W, Stoltze P and Nørskov J K 1996 *Surf. Sci.* **366** 394
[32] Finnis M W and Sinclair J E 1984 *Phil. Mag.* A **50** 45
[33] Sutton A P and Chen J 1990 *Phil. Mag. Lett.* **61** 139
[34] Daw M S and Baskes M I 1984 *Phys. Rev.* B **29** 6443
[35] Foiles S M, Baskes M I and Daw M S 1986 *Phys. Rev.* B **33** 7983
[36] Crampin S, Hampel K, MacLaren J M and Vvedensky D D 1990 *J. Mater. Res.* **5** 2107
[37] Rosengaard N M and Skriver H L 1993 *Phys. Rev.* B **47** 12 865
[38] Stokbro K and Jacobsen K W 1993 *Phys. Rev.* B **47** 4916
[39] Rasmussen T, Jacobsen K W, Leffers T and Pedersen O B 1997 *Phys. Rev.* B **56** 2977
[40] Rasmussen T 1998 *PhD Thesis* Technical University of Denmark
[41] Mills G, Jónsson H and Schenter G 1995 *Surf. Sci.* **324** 305
[42] Jónsson H, Mills G and Jacobsen K W 1998 *Classical and Quantum Dynamics in Condensed Phase Simulations* ed B J Berne, G Ciccotti and D F Coker (Singapore: World Scientific)
[43] Henkelman G, Uberuaga B and Jónsson H 2000 *J. Chem. Phys.* **113** 9901
[44] Friedel J 1957 *Dislocations and Mechanical Properties of Crystals* ed J C Fisher *et al* (New York: Wiley)
[45] Escaig B 1968 *Dislocation Dynamics* ed A R Rosenfeld, G T Hahn, A L Bement Jr and R I Jaffee (New York: McGraw-Hill)
[46] Seeger A 1957 *Dislocations and Mechanical Properties of Crystals* ed J C Fisher *et al* (New York: Wiley)
[47] Fleischer R L 1959 *Acta. Metall.* **7** 134
[48] Duesbery M S, Louat N P and Sadananda K 1992 *Acta. Metall. Mater.* **40** 149
[49] Püschl W and Schoeck G 1993 *Mater. Sci. Eng.* A **164** 286
[50] Saada G 1991 *Mater. Sci. Eng.* A **137** 177
[51] Rasmussen T *et al* 1997 *Phys. Rev. Lett.* **79** 3676
[52] Duesbery M S 1998 *Modell. Simul. Mater. Sci. Eng.* **6** 35
[53] Rao S, Parthasarathy T A and Woodward C 1999 *Phil. Mag.* A **79** 1167
[54] Stroh A N 1954 *Proc. Phys. Soc.* B **67** 427
[55] Bonneville J and Escaig B 1979 *Acta. Metall.* **27** 1477
[56] Bonneville J, Escaig B and Martin J L 1988 *Acta. Metall.* **36** 1989
[57] Rasmussen T *et al* 2000 *Phil. Mag.* A **80** 1273
[58] Hänggi P, Talkner P and Borkovec M 1990 *Rev. Mod. Phys.* **62** 251
[59] Voter A F and Doll J 1985 *J. Chem. Phys.* **82** 80
[60] Vegge T *et al* 2000 *Phys. Rev. Lett.* **85** 3866
[61] Stoltze P 1997 *Simulation Methods in Atomic-Scale Materials Physics* (Lyngby: Polyteknisk Forlag)
[62] Vegge T, Leffers T, Pedersen O B and Jacobsen K W 2001 *Mater. Sci. Eng.* A **319–321** 119
[63] Zhou S J, Preston D L, Lomdahl P S and Beazley D M 1998 *Science* **279** 1525
[64] Vegge T *et al* 2001 *Phys. Rev. Lett.* **86** 1546
[65] Hirsch P B 1962 *Phil. Mag.* **7** 67

[66] Hazif R L, Dorizzi P and Poirier J P 1973 *Acta. Mater.* **21** 903
[67] Bhatt R T, Thrower P A and Bitler W R 1976 *Scr. Metall.* **10** 19
[68] Pichaud B and Minari F 1980 *Scr. Metall.* **14** 1171
[69] Vegge T *et al* 2001 *Phil. Mag. Lett.* **81** 137
[70] Lothe J and Hirth J P 1959 *Phys. Rev.* **115** 543
[71] Seeger A and Schiller P 1962 *Physical Acoustics* vol 3A, ed W P Mason (New York: Academic) p 361
[72] Schottky G 1964 *Phys. Status Solidi* a **5** 697
[73] Joós B and Duesbery M S 1997 *Phys. Rev. Lett.* **78** 266
[74] Hikata A and Elbaum C 1985 *Phys. Rev. Lett.* **54** 2418
[75] Thompson E-J and Pohl R O 1999 *Mater. Res. Soc. Symp. Proc.* vol 562 (Warrendale, PA: Minerals, Metals and Materials Society) p 183
[76] Ralph D C, Ludwig A W W, von Delft J and Buhrman R A 1994 *Phys. Rev. Lett.* **72** 1064
[77] Vegge T, Pedersen O B, Leffers T and Jacobsen K W 2000 *Multiscale Phenomena in Materials—Experiments and Modeling* ed I M Robertson *et al (Mater. Res. Soc. Symp. Proc. vol 578)* (Warrendale, PA: Minerals, Metals and Materials Society) p 217
[78] Friedel J 1964 *Dislocations* (London: Pergamon)
[79] Argon A S and Moffatt W C 1981 *Acta. Metall.* **29** 293
[80] Zhou S J, Preston D L and Louchet F 1999 *Acta. Metall.* **47** 2695
[81] Carter C B 1979 *Phys. Status Solidi* a **54** 395
[82] Saka H, Kondo T and Kiba N 1981 *Phil. Mag.* A **44** 1213
[83] Schilling W 1978 *J. Nucl. Mater.* **69–70** 465
[84] Huang J, Meyer M and Pontikis V 1989 *Phys. Rev. Lett.* **63** 628
[85] Mishin Y *et al* 2001 *Phys. Rev.* B **63** 224106
[86] Young F W 1978 *J. Nucl. Mater.* **69–70** 310
[87] Siegel R W 1982 *Point Defects and Defect Interactions in Metals* ed J I Takamura, M Doyama and M Kiritani (Amsterdam: North-Holland) p 533
[88] Balluffi R W 1978 *J. Nucl. Mater.* **69–70** 241
[89] Carter C B 1980 *Phil. Mag.* A **41** 619
[90] M C T *et al* (ed) *Surface Diffusion (Proc. NATO Conf. ASI Series B vol 360)* (New York: Plenum)
[91] van Gastel R, Somfai E, van Saarloos S B and Frenken J W M 2001 *Phys. Rev. Lett.* **86** 1562
[92] Darby T P and Balluffi R W 1977 *Phil. Mag.* **36** 53
[93] Sorensen M R, Mishin Y and Voter A F 2000 *Phys. Rev.* B **62** 3658
[94] Nabarro F R N and de Villiers H L 1995 *The Physics of Creep* (London: Taylor and Francis)
[95] Balluffi R W 1970 *Phys. Status Solidi* **42** 11
[96] Huang J, Meyer M and Pontikis V 1990 *Phys. Rev.* B **42** 5495
[97] Hoagland R, Voter A and Foiles S 1998 *Scr. Mater.* **39** 589
[98] Ercolessi F and Adams J B 1994 *Europhys. Lett.* **26** 583
[99] Fang Q F and Wang R 2000 *Phys. Rev.* B **62** 9317
[100] Carling K and Wanström G 2000 *Phys. Rev. Lett.* **85** 3862
[101] Vegge T 2001 *PhD Thesis* Technical University of Denmark
[102] Wuttig M and Birnbaum K H 1966 *Phys. Rev.* **147** 495
[103] Balluffi R W and Granato A V 1979 *Dislocations in Solids* vol 4, ed F R N Nabarro (Amsterdam: North-Holland) p 1
[104] Huang J, Meyer M and Pontikis V 1991 *Phil. Mag.* A **63** 1149
[105] Winning M, Gottstein G and Shvindlerman L S 2001 *Acta. Mater.* **49** 211
[106] Essmann U and Rapp M 1973 *Acta. Metall.* **21** 1305
[107] Basinski Z S, Korbel A S and Basinski S J 1980 *Acta. Metall.* **28** 191
[108] Aslanides A and Pontikis V 2000 *Phil. Mag.* A **80** 2337
[109] Mughrabi H 2000 Private communication Institut für Werkstoffwissenschaften, Universität Erlangen-Nürnberg
[110] Tichy G and Essmann U 1989 *Phil. Mag.* A **60** 503
[111] Basinski Z S 1964 *Discuss. Faraday Soc.* **38** 93
[112] Fourie J T 1968 *Phil. Mag.* **17** 735
[113] Seeger A 1964 *Discuss. Faraday Soc.* **38** 82
[114] Antonopoulos J G, Brown L M and Winter A T 1976 *Phil. Mag.* **34** 549
[115] Wintner E and Karnthaler H P 1977 *Phil. Mag.* **36** 1317
[116] Wintner E and Karnthaler H P 1978 *Acta. Metall.* **26** 941
[117] Lim S-H *et al* 1998 *Phys. Rev. Lett.* **81** 5350
[118] Yonenaga I, Lim S-H, Lee and Shindo D 2001 *Mater. Sci. Eng.* A **309–10** 125